Journal of Civil Engineering and Urban Planning (2025)
Clausius Scientific Press, Canada

DOI: 10.23977/jceup.2025.070203
ISSN 2616-3969 Vol. 7 Num. 2

The Finite Element Analysis of Axial Compressive Behavior of Square CFST Columns with Multiple Localized Corrosions

Jing Li*

Key Laboratory of Urban Security and Disaster Engineering of Ministry of Education, Beijing University of Technology, Beijing, 100124, China
**Corresponding author*

Keywords: Square Concrete Filled Steel Tube Column; Multiple Localized Corrosion; Axial Compression Performance; Numerical Simulation

Abstract: Concrete filled steel tube can fully utilize the advantages of both steel and concrete, which is why it is widely used in high-rise buildings, airport stations, bridges, and other projects. However, during the long-term service life of CFST columns, corrosion is inevitably encountered. This paper uses finite element software to simulate the effects of multiple localized corrosion on square CFST columns. It analyzes the influence of various factors such as multiple localized corrosion depth, multiple localized corrosion shape, multiple localized corrosion circumferential position, and multiple localized corrosion axial height on the specimen's bearing capacity, stiffness, and ductility, revealing the degradation pattern of bearing capacity in square CFST with multiple localized corrosions. The research results show that as the depth of multiple localized corrosions increases, the bearing capacity of the specimen gradually decreases, and the rate of decrease accelerates. With the same corrosion area, the larger the axial length of the multiple localized corrosions, the greater its impact on the specimen's bearing capacity. As the angle of multiple localized corrosion increases, the specimen's bearing capacity first decreases and then increases. When two localized corrosions are on opposite sides, the weakening effect on bearing capacity is relatively small. When the two localized corrosions are adjacent to each other, the weakening effect on bearing capacity is more significant. When one corrosion is located at the midpoint of the column and the other at one-quarter of the column height, the specimen has the lowest bearing capacity, with a decrease of nearly 10% compared to the non-corroded specimen, and it is slightly lower than the specimen where the corrosion is uniformly located at the midpoint of the column height. When corrosion occurs at the bottom of the column, the weakening effect on bearing capacity is reduced due to the end effect.

1. Introduction

Concrete filled steel tubes (CFST) are widely used in engineering due to their high load-bearing capacity, excellent plasticity and toughness, and ease of construction.[1] However, during the long-

term service life of CFST structures, corrosion may occur as a result of environmental factors and other influences. The presence of corrosion inevitably leads to a decline in the mechanical properties of the specimens, resulting in economic losses, and in severe cases, may even cause engineering accidents.[2] To address this issue, scholars both domestically and internationally have conducted studies on the axial compressive performance of CFST columns through experimental tests, numerical simulations, and theoretical analyses.

CFST columns typically have either circular or square cross-sectional shapes. Regarding the research on the axial compressive performance of corroded circular CFST columns, Zhang et al.[3-4] conducted studies on the axial compressive performance of CFST columns subjected to freeze-thaw cycles and acid rain combined effects. Han et al.[5-6] investigated the performance of short circular CFST columns under sustained loading and chloride salt corrosion, using loading ratio and corrosion conditions as parameters. In addition, there has been research on localized corrosion. Huang et al. [7] conducted axial compressive tests on circular CFST short columns with artificial notches. Yu et al. [8] studied the effects of concrete strength, notch holes or grooves, and different loading conditions on column bearing capacity and load deformation. Li et al. [9] established a finite element model to study localized pitting corrosion in CFST columns. The model considered the randomness of the size, depth, and distribution of pitting corrosion pits, and validated the model using preliminary experimental data. Guo et al. [10] studied the axial compression performance of long columns with localized corrosion, with the main parameters being defect shape, defect size, and aspect ratio. Li et al. [10] conducted axial compression tests on low strength concrete with locally corroded steel tubes and found that the confinement effect of corroded steel tubes was reduced during specimen failure.

The above research involves general and localized corrosion of circular CFST columns, as well as general and localized corrosion of square CFST columns. Current research primarily focuses on the axial compressive performance of circular CFST columns, with relatively few studies examining the axial compressive behavior of square CFST short columns with localized corrosion. Among the limited studies, most have investigated the effects of a single localized corrosion. In real-life scenarios, multiple corrosion sites are more common, and their locations are more random. Therefore, research on the impact of multiple localized corrosion on the axial compressive performance of square CFST columns remains insufficient.

This study conducts a numerical simulation to investigate the effect of multiple localized corrosion on the axial compressive performance of square CFST short columns. It discusses the influence of parameters such as the localized corrosion depth, the localized corrosion shape, the localized corrosion circumferential position, and the localized corrosion axial height on the axial compressive strength and load-displacement curves of square CFST short columns.

2. Establishment of Finite Element Model

2.1 Constitution and Grid Division

Previous finite element studies have used different stress-strain models for steel, including the ideal elastoplastic model and the linear hardening elastoplastic model. However, the choice of different steel stress-strain models has little impact on the simulation results of the mechanical performance of CFST specimens. The material constitutive relationship of steel in this study adopts the elastoplastic model proposed by Tao et al.[11] in Figure 1. The model is divided into the elastic, plastic, strain-hardening, and secondary plastic flow segments. In the elastic segment, the elastic modulus of steel (Es) is taken as 200,000 MPa, and the Poisson's ratio (μ_s) is taken as 0.3. The specific expressions are as follows:

$$\sigma_s = \begin{cases} E_s\varepsilon & 0 \le \varepsilon_s < \varepsilon_y \\ f_y & \varepsilon_y \le \varepsilon_s < \varepsilon_p \\ f_u - (f_u - f_y)\cdot\left(\dfrac{\varepsilon_u - \varepsilon_s}{\varepsilon_u - \varepsilon_p}\right)^p & \varepsilon_p \le \varepsilon_s < \varepsilon_u \\ f_u & \varepsilon_u \le \varepsilon_s \end{cases} \tag{1}$$

Where f_y and f_u represent the yield strength and tensile strength of steel, respectively. E_p is the initial elastic modulus at the beginning of strain hardening, taken as $0.02E_s$. ε_y, ε_p and ε_u are the yield strain, the strain at the beginning of strain strengthening and the strain corresponding to the tensile strength, respectively. ε_p and ε_u can be calculated using the following equation:

$$\varepsilon_p = \begin{cases} 15\varepsilon_y & f_{y\le}300\text{MPa} \\ [15 - 0.018(f_y - 300)]\varepsilon_y & 300\text{MPa}<f_y \le 800\text{MPa} \end{cases} \tag{2}$$

$$\varepsilon_u = \begin{cases} 100\varepsilon_y & f_{y\le}300\text{MPa} \\ [100 - 0.15(f_y - 300)]\varepsilon_y & 300\text{MPa}<f_y \le 800\text{MPa} \end{cases} \tag{3}$$

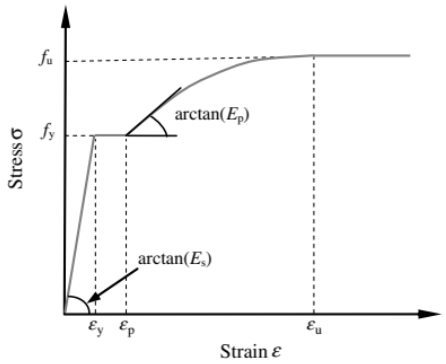

Figure 1: Stress strain relationship of steel

This study adopts the concrete constitutive model proposed by Han et al [12]. The specific expression is as follows:

$$y = \begin{cases} 2x - x^2 & x \le 1 \\ \dfrac{x}{\beta(x-1)^\eta + x} & x > 1 \end{cases} \tag{4}$$

Where: $x = \dfrac{\varepsilon}{\varepsilon_0}; y = \dfrac{\sigma}{\sigma_0}; \sigma_0 = f_c; \varepsilon_0 = \varepsilon_c + 800\zeta^{0.2}\times10^{-6}; \varepsilon_c = (1300 + 12.5f_c)\times10^{-6}$

$$\eta = 1.60 + 1.5/x; \beta = \frac{f_c^{0.1}}{1.2\sqrt{1+\zeta}}$$

Where f_c is the compressive strength of concrete cylinders; The elastic modulus of concrete $E_c = 4730\sqrt{f_c}$, MPa; Poisson's ratio μ_s, taken as 0.2.

In the numerical simulation, both the steel tube and the core concrete use 8-node solid elements

C3D8R. The top and bottom plates are modeled using 4-node discrete rigid shell elements R3D4. The meshing process affects the results of the finite element analysis. The larger the mesh size, the fewer the number of elements and the smaller the computational effort, but the accuracy of the results is poorer. Conversely, the smaller the mesh size, the more elements there are, and the results are relatively closer to the real situation, but the computational effort increases. Additionally, if the mesh size is too small, when the model experiences large deformations, the excessively small mesh may deform, leading to non-convergence of the model. For computational accuracy, the element size is controlled to be $B/15$, where B is the side length of the specimen.

2.2 Contact type and boundary conditions

In the finite element model, the interaction between components is achieved by defining contact. For CFST components, it is necessary to define the interactions between the internal concrete and the external steel tube, the interaction between the concrete and the end plates, and the interaction between the steel tube and the end plates. The contact type between the steel tube and concrete, as well as between the end plates and concrete, is surface-to-surface. The contact surface is modeled with hard contact in the normal direction and penalty contact in the tangential direction, with a friction coefficient of 0.6. The contact type between the steel tube and the end plates is a tie constraint. The boundary conditions are set as follows: rotation restraint is released in the X-direction, and full restraint is applied in the other directions.

3. Parameter design and analysis

3.1 Parameter design

The basic parameters for the finite element model parameter analysis are as follows: specimen length L=450 mm, specimen side length B=150 mm, steel tube thickness t=4 mm, and localized corrosion position 1: half of the column height. The yield strength f_y of steel tube and the compressive strength f_{cy}150 of concrete are 345MPa and 50MPa, respectively. There are four research variables: corrosion depth, corrosion shape, corrosion axial height, and corrosion circumferential position. Among them, d represents the corrosion depth, with two conditions set at 2 mm and 4 mm. l and b represent the length of the localized corrosion along the column height and the width of the localized corrosion, respectively. l/b represents the corrosion shape, with four conditions set at 0.25, 1, 2.25, and 4. α represents the angle between the line connecting the centroid of corrosion and the section center, with two conditions set at 90 °and 180 °, which correspond to adjacent and opposite corrosion positions, respectively. l/L represents the relative position of localized corrosion 2 along the axial direction of the CFST column, with three conditions set at 1/2, 1/4, and 1/12, indicating that the corrosion is located at half the column height, a quarter of the column height, and at the bottom of the column, respectively. The reduction coefficient of bearing capacity $\varphi=N/N_0$ represents the influence of multiple localized corrosions on the bearing capacity of the specimen. The specimen naming convention is as follows: the multiple localized corrosion circumferential position - the multiple localized corrosion depth - the multiple localized corrosion shape - the multiple localized corrosion axial height. For example, 180-4-1-1/2 indicates that two localized corrosions are located on opposite sides, with a corrosion depth of 4 mm, a square corrosion shape, and both localized corrosions positioned at half the column height.

3.2 Failure mode

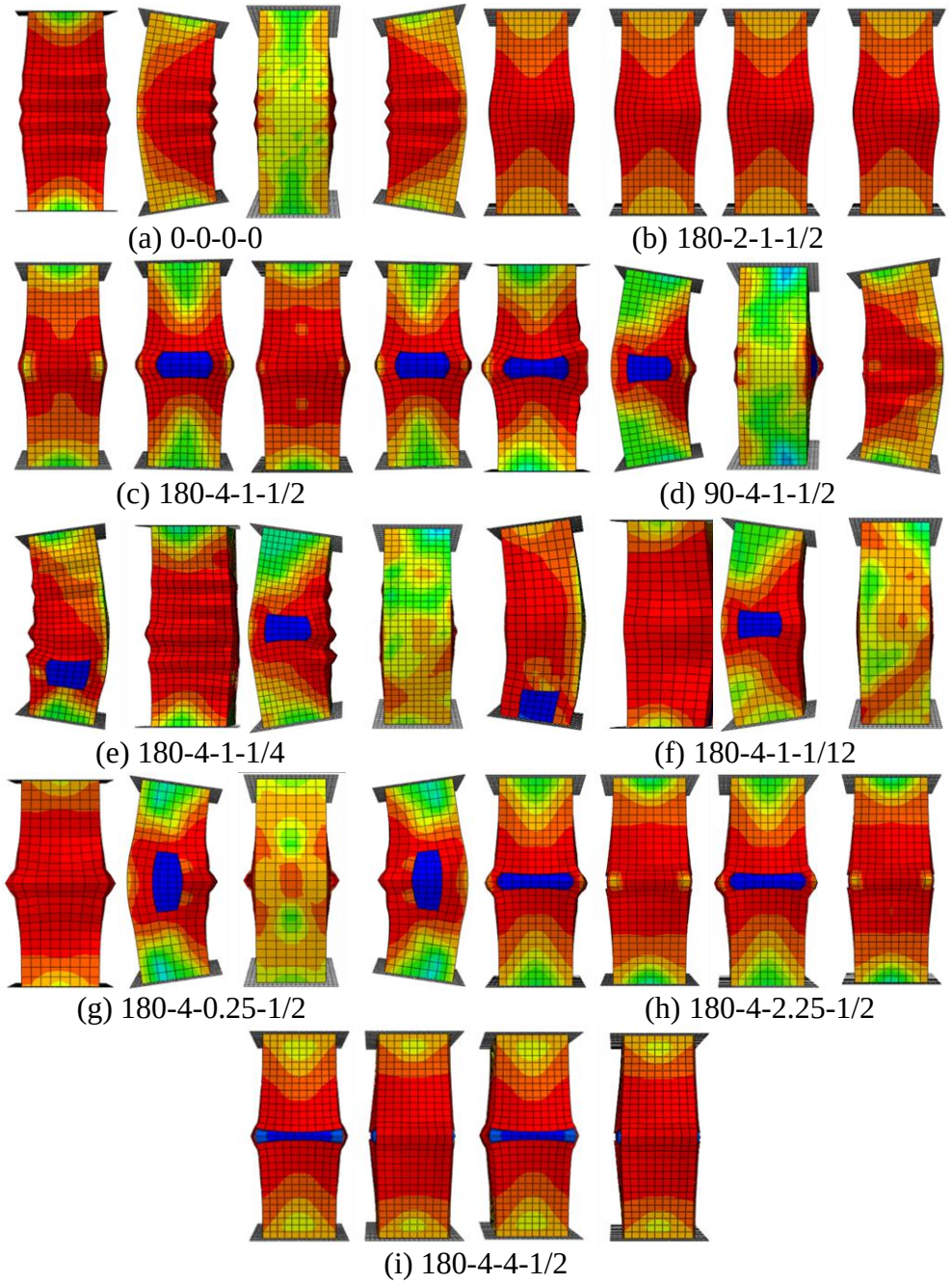

Figure 2. Failure mode diagram of the specimen

By performing finite element analysis of the failure modes of specimens under different parameters of localized corrosion, a better understanding of the impact of localized corrosion on structural performance can be achieved. By analyzing the force distribution and localized deformation of the columns, the failure mode and mechanism of the specimens can be predicted. Designers can identify which parts are most susceptible to corrosion, thus optimizing design and reinforcement measures. At the same time, finite element analysis can simulate the mechanical behavior of corrosion-damaged CFST columns in a computer, reducing the need for experimental studies and saving a significant amount of experimental costs and time. Overall, this not only helps improve the safety and durability

of the structure but also effectively reduces maintenance costs and provides scientific support for anti-corrosion design and construction.

Figure 2 shows the front view, left view, rear view, and right view of the failure modes of each specimen. Figure 2 (a) indicates that the failure mode of the uncorroded CFST column is skewed to one side. This is because, when the column is subjected to axial loads, the stress distribution between the steel tube and the concrete is usually uneven. However, after adding symmetric corrosion, the stress distribution and failure process are altered, making the failure mode of the column more stable and preventing the skewed failure caused by asymmetry. It is worth noting that in Figure 2 (g), the failure mode of the specimen is also asymmetric. This may be because the localized corrosion with a large axial length does not change the originally uneven stress distribution of the specimen.

As can be seen from Figure 2 (b)-(c), the greater the corrosion depth, the more pronounced the local buckling of the specimen. Figure 2 (c), (g)-(i) show that the larger the *l/b* ratio, the smaller the impact of localized corrosion on the failure mode of the specimen, making the specimen more stable. Figure 2 (c)-(d) indicate that localized corrosion at adjacent positions makes the specimen more unstable, resulting in larger deformations. Figure 2 (c), (e)-(f) show that corrosion at half the column height and one-quarter of the column height causes the most severe deformation in the specimen.

3.3 Parameter analysis

3.3.1 The effect of multiple localized corrosions depth

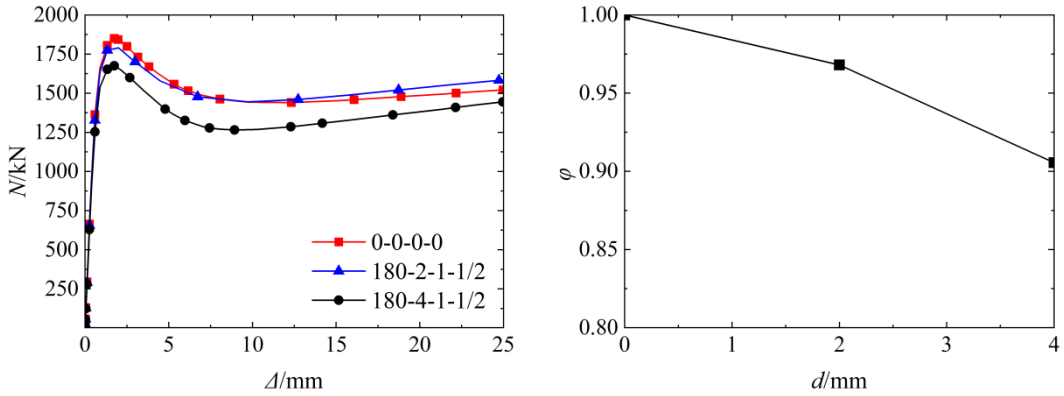

Figure 3: The influence of multiple localized corrosion depth

The effect of multiple localized corrosions depth on the load-displacement curve and bearing capacity of CFST columns is shown in Figure 3. From Fig 3, it can be seen that the multiple localized corrosions depth does not affect the slope of the load-displacement curve, meaning the stiffness of the specimen does not decrease. As the multiple localized corrosions depth increases, the bearing capacity of the specimen gradually decreases. When the multiple localized corrosions depth is less than half of the steel tube thickness, the bearing capacity decreases slowly. When the multiple localized corrosions depth exceeds half of the steel tube thickness, the bearing capacity decreases more rapidly. This is because the greater the multiple localized corrosions depth, the weaker the restraining effect of the steel tube on the core concrete, resulting in a significant decrease in the bearing capacity of the specimen.

3.3.2 The effect of multiple localized corrosions shape

Figure 4 shows the load-displacement curves and bearing capacity curves of square CFST columns with different shapes of multiple localized corrosions. From the figure, it can be seen that multiple

localized corrosions shape affect the bearing capacity and ductility of the CFST columns. As the ratio of *l/b* increases from 0.25 to 4, the bearing capacity of the specimen gradually decreases. That is, with the same area, the greater the axial length of localized corrosion, the greater its impact on the specimen's bearing capacity. It is worth noting that specimen 180-5-0.25-1/2 shows a decrease after reaching the peak bearing capacity and then remains constant, while other specimens show a decrease followed by a slight increase after reaching the peak bearing capacity.

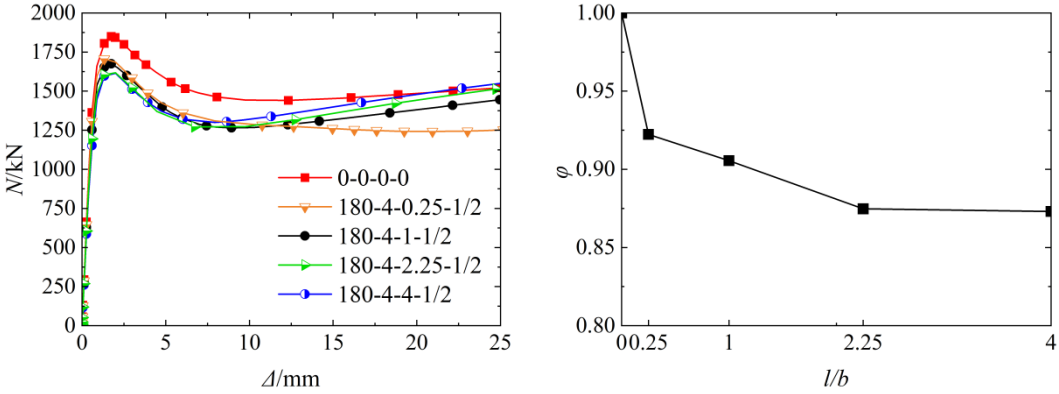

Figure 4: The influence of multiple localized corrosions shape

3.3.3 The effect of multiple localized corrosions circumferential position

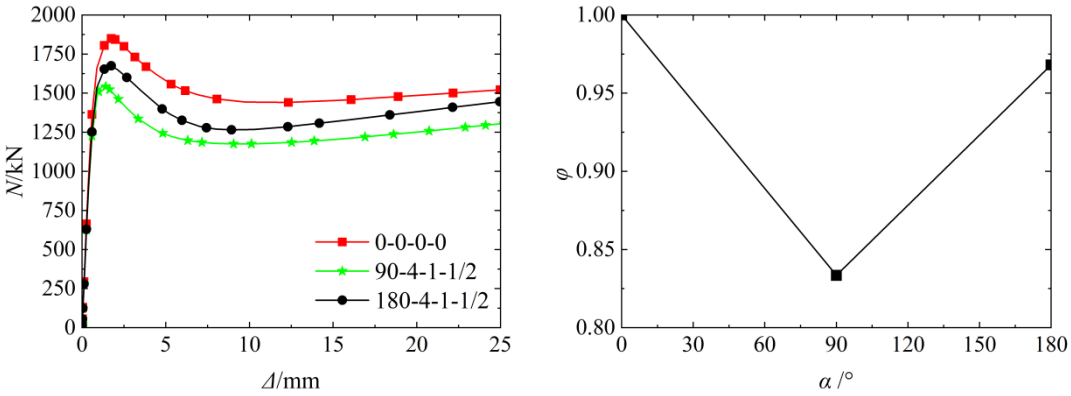

Figure 5: The influence of multiple localized corrosions circumferential position

By changing the circumferential position of localized corrosion and altering the arrangement of the two localized corrosion from a symmetric layout ($a = 180^{\circ}$) to an asymmetric layout ($a = 90^{\circ}$), the impact of corrosion-induced changes in the centroid position on the axial compressive bearing capacity of the specimen can be studied. As shown in Figure 5, as the relative angle of corrosion increases, the specimen's bearing capacity first decreases and then increases. When the two local corroded areas are on opposite sides, the weakening effect on the bearing capacity is small, with a decrease in bearing capacity of less than 5%. However, when the two local corroded areas are adjacent, the weakening effect on the bearing capacity is more significant, with a decrease in bearing capacity of over 15%, making the impact non-negligible. Overall, the axial compressive bearing capacity of the asymmetric specimens is reduced by nearly 10% compared to the symmetric specimens, indicating a significant impact.

3.3.4 The effect of multiple localized corrosions axial height

From Figure 6, it can be seen that the variation in the axial position of corrosion has an impact on the specimen. When two corroded areas are located at one-half and one-quarter of the column height, the specimen exhibits the lowest load-bearing capacity, which is nearly *a* 10% reduction compared to the uncorroded specimen. The load-bearing capacity is also slightly lower than that of the specimen with corrosion at the half-height of the column. This may be due to the asymmetric distribution of corrosion, which has a greater impact on the structural forces and stability, leading to a lower load-bearing capacity compared to specimens where both corrosion areas are located at the column's half-height. In the finite element simulation, such an asymmetric corrosion distribution may lead to more complex stress distributions and local buckling behaviors, thereby affecting the overall load-bearing capacity. When corrosion is located at the bottom of the column, the weakening effect on the specimen's load-bearing capacity is reduced due to the end effect. Therefore, the load-bearing capacity of specimen 180-4-1-1/12 is the highest among the corroded specimens.

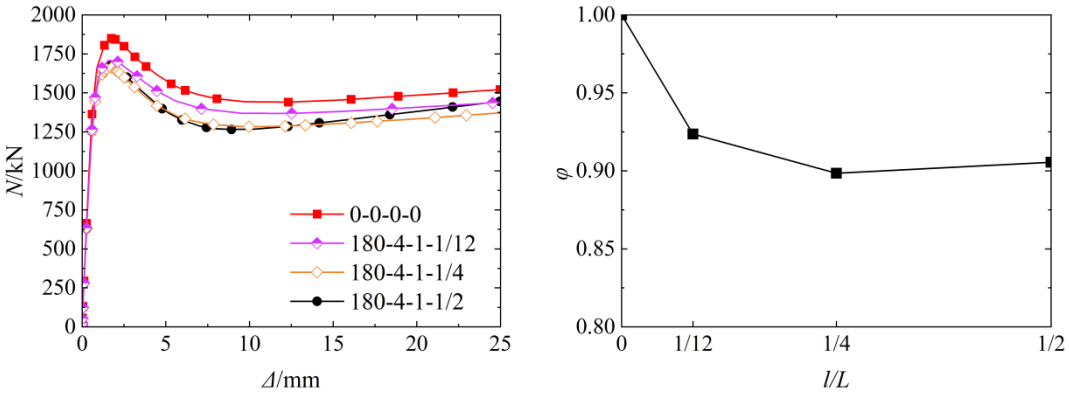

Figure 6: The influence of multiple localized corrosions axial height

4. Conclusions

This study established an ABAQUS finite element model for analyzing the bearing capacity of CFST columns with multiple localized corrosions under axial load. The effects of multiple localized corrosions depth, multiple localized corrosions shape, multiple localized corrosions circumferential position, and multiple localized corrosions axial height on the axial performance of the CFST columns were analyzed. The following conclusions were drawn from the analysis:

(1) Within the parameter range of this study, as the corrosion depth increases, the bearing capacity of the specimens gradually decreases.

(2) Under the same corrosion area, localized corrosion with different shapes has different effects on the bearing capacity of the specimens. The larger the axial length of localized corrosion, the greater its impact on the bearing capacity of the specimen.

(3) Symmetrically arranged localized corrosion has a small impact on the bearing capacity of the specimen, while asymmetrically arranged localized corrosion significantly reduces the bearing capacity.

(4) Changes in the axial height of localized corrosion affect the degree of bearing capacity degradation. Among the corroded specimens, when the localized corrosion of specimen 2 is located at the bottom of the column, the bearing capacity is highest due to the end effect. When the localized corrosion of specimen 2 is located at one-quarter of the column height, the bearing capacity is lowest due to the asymmetric distribution of corrosion.

References

[1] Ma H, Dong J, Liu Y, and Guo T`. Compressive behaviour of composite columns composed of RAC-filled circular steel tube and profile steel under axial loading. Journal of Constructional Steel Research. 2018; 143: 72-82.
[2] Wu ZQ, Wei Y, Wang XT, et al. Orthogonal experimental study in axial mechanical behavior of locally corroded circular steel tubes. Engineering mechanics. 2020; 37: 144-152.
[3] Zhang T, Lyu X, Yu Y. Prediction and analysis of the residual capacity of concrete-filled steel tube stub columns under axial compression subjected to combined freeze–thaw cycles and acid rain corrosion [J].Materials, 2019, 12(19):3070.
[4] Zhang T, Lyu X, Yu Y. Degradation of Axial Ultimate Load-Bearing Capacity of Circular Thin-Walled Concrete-Filled Steel Tubular Stub Columns after Corrosion[J]. Materials, 2020, 13(3):795.
[5] Han LH, Hou C, Wang QL. Square concrete filled steel tubular (CFST) members under loading and chloride corrosion: Experiments [J]. Journal of Constructional Steel Research, 2012, 71:11-25.
[6] Han LH, Hou CC, Wang QL. Behavior of circular CFST stub columns under sustained load and chloride corrosion [J].Journal of Constructional Steel Research, 2014, 103:23-36.
[7] Huang HJ, Guo LH, Qu B, Jia C, and Elchalakani M. Tests of circular concrete-filled steel tubular stub columns with artificial notches representing local corrosions. Engineering Structures. 2021; 242: 112598.
[8] Yu ZW, Ding FX, Cai C. Experimental behavior of circular concrete-filled steel tube stub columns[J].Journal of constructional steel research, 2007, 63(2):165-174.
[9] Li G, Hou C, Shen LM, et al. Performance and strength calculation of CFST columns with localized pitting corrosion damage[J].Journal of Constructional Steel Research, 2022, 188:107011.
[10] Guo LH, Li JW, Jia C, et al. Axial compression behavior of slender concrete-filled steel tubes with machining defects representing local corrosion [J].Engineering Structures, 2023, 286: 116091.
[11] Tao Z, Uy B, Liao FY, et al. Nonlinear analysis of concrete-filled square stainless steel stub columns under axial compression[J].Journal of Constructional Steel Research, 2011, 67(11):1719–1732.
[12] Han LH. Steel Tube Concrete Structures-Theory and Practice [M].Beijing: Science Press, 2004:66-92